High-Transconductance Organic Thin-Film Electrochemical Transistors for Driving Low-Voltage Red-Green-Blue Active Matrix Organic Light-Emitting Devices

Daniele Braga, Nicholas C. Erickson, Michael J. Renn, Russell J. Holmes, and C. Daniel Frisbie**

Switching and control of efficient red, green, and blue active matrix organic light-emitting devices (AMOLEDs) by printed organic thin-film electrochemical transistors (OETs) are demonstrated. These all-organic pixels are characterized by high luminance at low operating voltages and by extremely small transistor dimensions with respect to the OLED active area. A maximum brightness of ≈900 cd m^{-2} is achieved at diode supply voltages near 4 V and pixel selector (gate) voltages below 1 V. The ratio of OLED to OET area is greater than 100:1 and the pixels may be switched at rates up to 100 Hz. Essential to this demonstration are the use of a high capacitance electrolyte as the gate dielectric layer in the OETs, which affords extremely large transistor transconductances, and novel graded emissive layer (G-EML) OLED architectures that exhibit low turn-on voltages and high luminescence efficiency. Collectively, these results suggest that printed OETs, combined with efficient, low voltage OLEDs, could be employed in the fabrication of flexible full-color AMOLED displays.

1. Introduction

There is currently substantial interest in identifying thin-film transistor (TFT) technologies that provide sufficient drive currents and operational stability to meet the requirements of active matrix organic light-emitting devices (AMOLEDs).[1] Unfortunately, due to both low charge carrier mobility and bias stress effects, amorphous-Si TFTs that are ubiquitous in the backplanes of liquid crystal displays (LCDs) generally cannot deliver adequate currents to stably illuminate AMOLEDs. Consequently, commercial AMOLED displays typically employ glass backplanes with higher mobility and higher transconductance polycrystalline Si (poly-Si) drive circuitry. Alternatives to poly-Si circuitry are desirable from both cost and processing perspectives. For example, amorphous oxide or organic TFTs processed at low temperature (e.g., <150 °C) might allow roll-to-roll manufacturing of flexible AMOLED displays on plastic substrates that cannot withstand the high temperatures necessary for preparing poly-Si films.[2]

There have already been several different demonstrations of OLED, liquid crystal, electrophoretic, and electrochromic displays driven by organic TFT (OTFT) backplanes.[3–13] This prior work has highlighted the potential of OTFTs for display applications, but it also delineates some important problems, particularly with respect to driving AMOLED displays. So far, OTFTs are operationally and environmentally less stable than polycrystalline-Si TFTs and are unable to provide the same output current per unit channel width because of the lower charge carrier mobility (0.1–1 $cm^2\ V^{-1}s^{-1}$) in the organic semiconductor.[14] As a result of the relatively low mobility, high biases, and large OTFT footprints (areal sizes) are required to properly drive individual light-emitting pixels.[15] Large OTFT dimensions potentially limit the pixel resolution achievable with a fully organic technology. Indeed, a key figure of merit for AMOLED drive TFTs is the transconductance per unit channel width, which should be >100 μS cm^{-1} in order that the TFT footprint is not too large compared to the pixel dimensions.

We have recently demonstrated that electrolyte-gated OTFTs,[16] also referred to as microelectrochemical transistors,[17,18] can have transconductances on the order of 10 mS cm^{-1}, well above the required threshold. The architecture of these OTFTs, which employ a polymer electrolyte or "ion gel" as the gate dielectric, is shown in **Figure 1**a. When a gate voltage is applied, ions from the gate dielectric penetrate the polymer semiconductor layer, effectively electrochemically doping it and creating a high conductance state. Current flows throughout the thickness of the semiconductor layer, so that the conducting

Dr. D. Braga, Prof. R. J. Holmes, Prof. C. D. Frisbie
Department of Chemical Engineering and Materials Science
University of Minnesota
421 Washington Ave. SE, Minneapolis, MN 55455, USA
E-mail: rholmes@umn.edu; frisbie@umn.edu
N. C. Erickson
Department of Electrical and Computer Engineering
University of Minnesota
200 Union Street SE, Minneapolis, MN 55455, USA
Dr. M. J. Renn
Optomec, Inc. 1000 Westgate Dr.,
St. Paul, MN 55114, USA

DOI: 10.1002/adfm.201102075

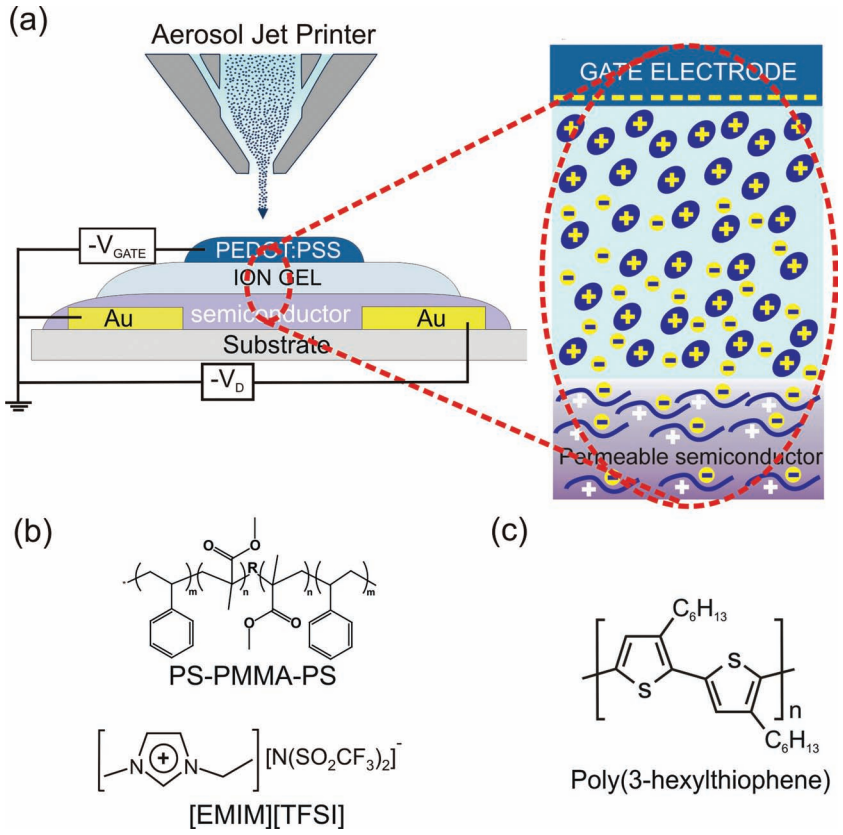

Figure 1. a) Cross section of a printed OET. When a negative gate voltage is applied, the semiconductor is electrochemically doped by anions from the electrolyte creating a high conductance channel. b) Molecular structures of the components of the electrolyte dielectric and c) semiconductor (P3HT). The ion-gel dielectric is a solid electronic insulator made by a gelating triblock copolymer (poly(styrene-*b*-methylmethacrylate-*b*-styrene (PS-PMMA-PS) swollen with an ionic liquid (1-ethyl-3-methylimidzaolium bis(trifluoromethylsulfonyl)imide ([EMIM][TFSI])).

channel is much thicker than in a conventional TFT. Resetting the gate bias to 0 V causes the electrochemical doping process to reverse. Effective gate capacitances are typically ≈10 μF cm^{-2},[16,19] and consequently very large channel currents can be obtained even for low mobility semiconductors, which is an advantage for application of these devices in OLED pixel control.

One potential issue concerning the use of organic thin-film electrochemical transistors (OETs) for OLED pixel backplanes is the OET switching time, which could be assumed to be rather long given that ions must be alternatively injected and withdrawn from the channel.[20] Fortunately, this switching time can be managed by controlling the thickness of the polymer semiconductor and the electrolyte layer. Previously, we have demonstrated 1 ms switching time for OETs employing the benchmark polymer semiconductor poly(3-hexylthiophene) (P3HT),[21] and 20 μs for OETs with semiconducting carbon nanotube channels.[22] 20 μs delay times are sufficient for video rate displays and we believe further improvements in switching speed can be made, perhaps large enough that 1 MHz switching frequencies could be obtained.[23]

A second consideration is the match between the OET and OLED operating voltages. In general, OETs cannot sustain applied gate-source or drain-source biases above ±3 V due to both electrolyte breakdown[24] and irreversible oxidation/reduction of the semiconductor.[25] Thus, while the low voltage characteristics of OETs are often considered to be an advantage, for AMOLED backplane applications the low voltage could potentially limit pixel brightness.

In this paper, we demonstrate for the first time that printed OETs can serve as switching and driving TFTs for red, green, and blue AMOLED pixels. The pixels are operated at high brightnesses up to 900 cd m^{-2} and are switched at rates up to 100 Hz. Furthermore, due to the high transconductance of the OETs, the pixel-to-transistor area ratio is >100:1, which is important from a display architecture and brightness perspective. Key to this demonstration is the use of vacuum deposited OLEDs that operate at 3–4 V by virtue of a novel single layer architecture previously reported.[26] The low voltage characteristics of the OLEDs mean that low pixel supply biases can be utilized that are compatible with the OET requirements. Indeed, in both the ON and OFF states of the pixels, only a fraction of the bias between the transistor source electrode and the OLED cathode drops over the drive transistor. This prevents electrolyte breakdown and the degradation of the OET performance. Collectively, the results suggest that OETs are promising candidates for the backplanes of printed AMOLED displays.

2. Characteristics of OETs and OLEDs

Staggered electrolyte-gated OTFTs were fabricated by aerosol jet printing following previously reported procedures (see Figure 1a).[16,21] The dielectric layer, formed by a gelating triblock copolymer [poly(styrene-*b*-methylmethacrylate-*b*-styrene)] and a room temperature ionic liquid (1-ethyl-3-methylimidazolium bis(trifluoromethylsulfonyl)imide ([EMIM][TFSI])) (Figure 1b), was printed on top of a P3HT semiconducting thin film (Figure 1c). Gold and the conducting polymer poly(3,4-ethylenedioxythiophene):poly(styrenesulfonate) (PEDOT:PSS) were used as source/drain and gate electrodes, respectively. When a negative bias is applied to the gate electrode, ions penetrate the semiconducting layer, oxidizing it and creating a high conductance channel between the source and drain electrodes. At the same time part of the PEDOT:PSS is reduced to a lower conductance state. Unwanted effects related to the decrease of the PEDOT:PSS conductance are avoided by employing a highly conductive PEDOT:PSS electrode exceeding the channel layer in thickness and lateral dimension.

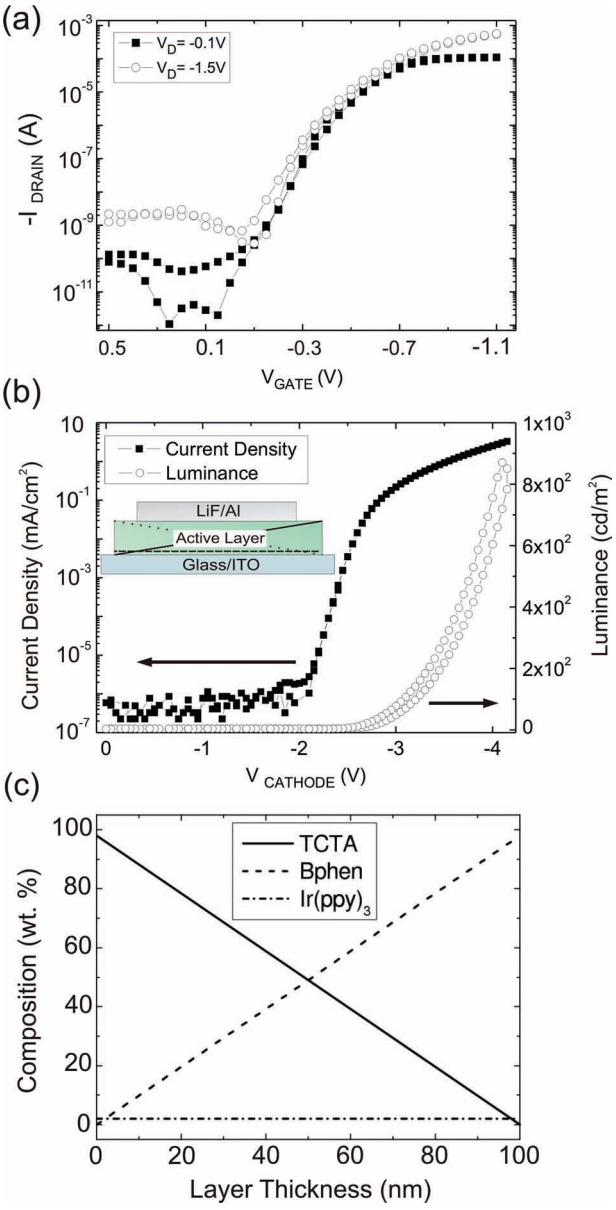

Figure 2. a) Quasi-equilibrium transfer characteristics of a gel-electrolyte gated organic transistor in linear ($V_D = -0.1$ V) and saturation ($V_D = -1.5$ V) regimes (sweep rate = 50 mV s^{-1}). Transistor channel length (L) and width (W) are L = 10 μm and W = 100 μm, respectively. b) Quasi-equilibrium current–voltage and luminance–voltage characteristics for a green G-EML OLED. In the forward regime the Al cathode is negatively biased relative to the indium tin oxide (ITO) anode. The inset in b shows the geometry of the OLED. c) Scheme of the spatial composition of the green G-EML OLED. The anode is at 0 nm while the cathode is at 100 nm. The composition of the phosphor is kept constant at 2 wt% throughout the structure.

Figure 2a displays the quasi-equilibrium transfer characteristics of an OET in the linear (drain voltage V_D = –0.1 V) and saturation (V_D = –1.5 V) regimes. Unique features of this device are high p-type transconductance, low hysteresis, low subthreshold voltage slope and low turn-on voltage ($V_{ON} \approx 0$ V). Moreover, the transistors are reasonably stable under gate voltage stress[27] and there is good uniformity between the characteristics of different devices printed on the same substrate.[16,21] These properties, together with the low parasitic resistance at the injecting/extracting contacts[28] and the absence of short channel length effects,[29] meet several requirements for the fabrication of high resolution active matrix light-emitting displays.[30]

It is important to point out that OETs exhibit relatively high OFF-state leakage current. In Figure 2a we see that the level of the OFF-current is reasonably low when the transistor operates in the linear regime (low V_D), but that the current increases when high voltage is applied between the source and drain electrodes. The cause of this is under investigation and may be related to water or impurities in the electrolyte (the devices are printed in air). High OFF currents can in principle cause problems for displays, e.g., poor pixel contrast control and high power consumption. However, wiring an OET in series with an efficient OLED that itself has high OFF state resistance can mitigate this problem. Furthermore, even for silicon backplanes leakage is a common issue, and different circuit designs have been implemented to bypass it.[31–33] The standard two-transistor active matrix can be replaced, for example, by a three-transistor geometry in which leakage current effects are significantly minimized.[34]

For light emission, we employed bottom-emission OLEDs comprising a single-layer, graded-composition emissive layer architecture (G-EML).[26] Typical current density–voltage and luminance–voltage characteristics are shown in Figure 2b with a schematic of the single-layer OLED shown in the inset. The G-EML contains a high concentration of hole transport material at the anode and electron transport material at the cathode with a continuously varying composition across the active layer. The phosphorescent guest is uniformly doped throughout the structure, shown schematically for a green G-EML OLED in Figure 2c. This device architecture exhibits low leakage currents (<1 nA cm^{-2}) and high external quantum efficiency (EQE) as a result of a high degree of charge confinement. Additionally, the G-EML devices show low turn-on voltages of ≈2.6 V and steep luminance–voltage characteristics leading to high luminance at low voltage (≈900 cd m^{-2} at 4.2 V). The combination of low leakage currents and steep current density–voltage dependence lead to high rectification ratios (≈10^5 at ±3 V) for the G-EML OLEDs.

3. OET-Driven OLED Pixels

3.1. Quasi-Equilibrium Characteristics

In order to examine the suitability of OETs for light-emitting display applications, we first characterized integrated devices made by a single stand-alone transistor placed in series with the OLED. The transistor that drives the light-emitting unit in a display is the most prone to fast degradation. Indeed, the driver must support part of the supply voltage (V_{DD}), i.e., the bias between the transistor source electrode and the diode cathode. The required V_{DD} depends on the OLED efficiency, on the characteristics of the transistor (mainly its transconductance), and on the brightness level that must be achieved. V_{DD} is commonly

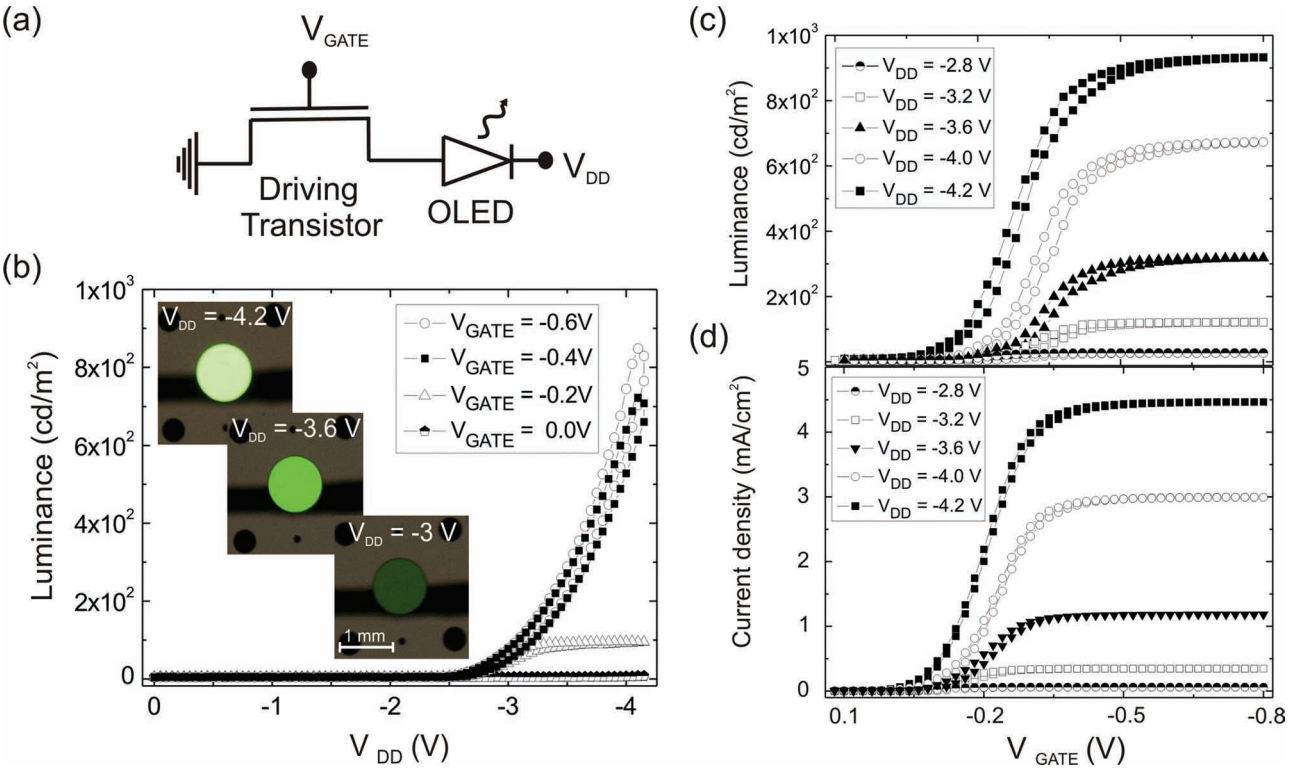

Figure 3. Optical and electrical characteristics of an OET/OLED integrated device using a green G-EML OLED. a) Circuit diagram showing the driver TFT in series with the light-emitting unit. b) Luminance vs. supply voltage (V_{DD}) at different gate voltages (V_{GATE}) and c) luminance vs. gate voltage at different V_{DD}. d) Current density at the OLED cathode versus V_{GATE} for different V_{DD}. Transistor channel length and channel width are $L = 20$ µm and $W = 200$ µm. The diameter of the OLED is $d = 1$ mm. In the inset of (b) pictures of the light-emitting unit at different brightness are also reported.

greater than the electrochemical stability window of electrolytes (approximately ±3 V), which is a potential problem for OETs.

A single OET (W/L = 10) was connected in series with an OLED (1 mm diameter), as indicated in the circuit diagram of **Figure 3**a. The optical and electrical characteristics of the integrated device are reported in Figure 3b–d as a function of V_{DD} and driving voltage (V_{GATE}). Pictures in the inset of Figure 3b show the optical output of a green OLED driven by a single OET at different V_{DD} values and with the same gate voltage (V_{GATE} = –0.6 V).

From Figure 3b, where the OLED luminance is reported versus the supply voltage at different gate voltages, we note that low supply voltages are sufficient to properly drive the OLED. Green G-EML OLEDs can be driven with an OET up to ≈900 cd m^{-2} with sub-1 V gate voltages and with a supply voltage V_{DD} = –4.2 V, as shown. This brightness level fully satisfies the requirement for indoor display applications and it is the same level that can be reached with the stand-alone OLED at the same applied voltage ($V_{CATHODE} = V_{DD}$). Thus, the OET is not the current bottleneck for the integrated device. Indeed, by comparing Figure 3b with the luminance–voltage characteristics of the stand-alone diode (Figure 2b), we note that when the transistor is fully ON (V_{GATE} = –0.6 V) there are no differences between the luminance vs. supply voltage response of the stand-alone OLED and the integrated device.

Figure 3c,d show the dependence of luminance and OLED current density on gate voltage for different fixed V_{DD} values. When the driving transistor is gated with low negative or positive biases, the OLED brightness is significantly suppressed, as expected, Figure 3c. The limit of zero light emission is achieved when the gate electrode is grounded and maintained when a low positive gate bias is applied. A sharp increase in the luminance is observed when the gate voltage is swept negatively with $V_{DD} > -3$ V. Indeed, the OET turns ON abruptly, because of the extremely low sub-threshold swing and properly drives the OLED at gate voltages smaller than –1 V. At sufficiently high V_{GATE} the OLED luminance saturates to the maximum brightness of the stand-alone OLED at $V_{CATHODE} = V_{DD}$. The OLED current density also saturates and follows the same trend as the luminance data (compare Figure 3c,d). In this case, the optical responses of the stand-alone OLED and of the integrated device are exactly the same and the output current of the transistor exceeds what is required to drive the diode at the given supply voltage. In other words, the saturation of the luminance versus V_{GATE} characteristics and current density versus V_{GATE} characteristics in Figure 3c,d indicate that the OLED, and not the OET, limits the current, as is desired.

3.2. Device Operation Mechanism and Geometrical Scaling

The satisfactory operation of the integrated OET/OLED device for supply voltages as large as V_{DD} = –4.2 V is initially somewhat surprising, as the voltage might be expected to cause

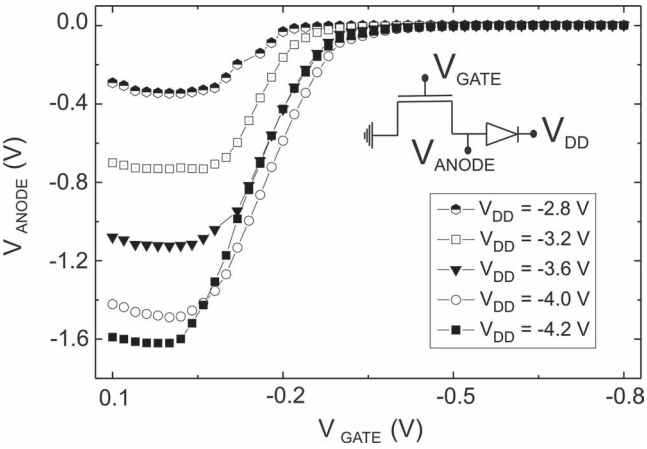

Figure 4. Voltage drop at the transistor/OLED common electrode (V_{ANODE}) vs. gate voltage (V_{GATE}) at different V_{DD}. During operation of the integrated device most of the applied V_{DD} drops on the OLED, preventing degradation of the electrolyte-gated transistor. A diagram of the circuit is shown in the inset. Maximum leak current in the OFF state is also limited by the diode.

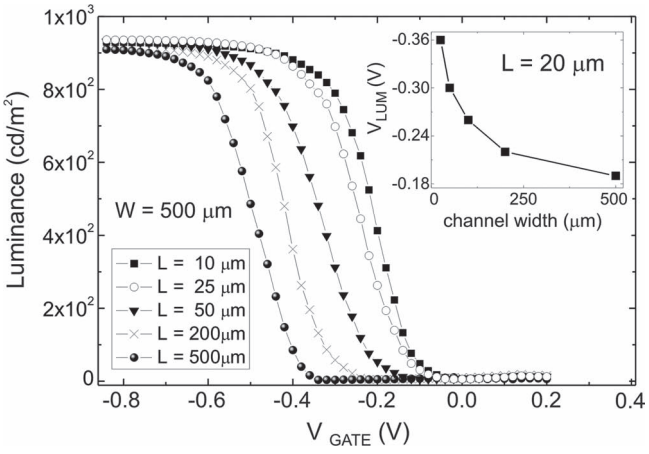

Figure 5. Luminance vs. gate voltage characteristics for different OET/OLED devices made with transistors having different channel lengths (L) and the same channel width (W). In the inset, the turn-on voltage of the optical output (V_{LUM}) is reported as a function of channel width for OETs with the same channel length. All measurements were carried out at constant supply voltage V_{DD} = –4.2 V. The light-emitting unit is a green G-EML OLED with a diameter of 1 mm.

breakdown of the gate electrolyte in the OET. However, it turns out that the effective voltage drop across the OET is always <|–2 V|. This can be seen in **Figure 4**, where we report the voltage drop at the transistor/OLED common electrode (V_{ANODE}) versus gate voltage at different supply voltages V_{DD}. It is evident that at negative V_{GATE}, when the driver transistor is ON, the supply voltage V_{DD} drops exclusively on the OLED and zero potential is recorded at the common electrode (V_{ANODE} = 0 V). On the other hand, when the gate voltage is swept positively to achieve the pixel OFF state, V_{ANODE} gradually transitions from ground to a finite value that depends on V_{DD}. The OFF state is the operation regime in which OET degradation could occur. However, even at a supply voltage of –4.2 V (corresponding to ≈900 cd m^{-2}) only a fraction of V_{DD} drops on the TFT. This is because the transistor OFF-state is characterized by a non-negligable leakage current (Figure 2a), so that the voltage drop across the OET is smaller than for an ideal transistor with negligible leakage. At a supply of voltage of V_{DD} = –4.2 V, the maximum potential difference between the transistor source and drain electrodes is ≈1.6 V, a voltage value that is far below the limit imposed by the electrochemical window of the employed electrolyte. Previously reported studies have demonstrated that when sub-2 V voltages are employed, OETs are reasonably stable under gate bias stress and after several hours of dynamic operation.[16,27] Note that OFF-state leakage current through the integrated device is limited by the diode, and proper sizing of the OLED and OET components can minimize OFF-state power dissipation.

We also examined how the dimensions of the driver TFT influence the performance of the integrated device. Our purpose is to show that the transistor footprint is not a limiting factor for the fabrication of high-resolution active matrix displays. The same OLED was driven by two sets of different OETs: transistors with the same channel width (W = 500 μm) but different channel lengths (10 μm ≤ L ≤ 500 μm), and transistors with the same channel length (L = 20 μm) but different channel width (20 μm ≤ W ≤ 500 μm). **Figure 5** shows the luminance–voltage characteristics of integrated devices made with transistors of different channel length. In the inset of Figure 5, we also report the onset of light emission (V_{LUM}) versus the width of the TFT channel. Data reported in the inset refer to transistors with the same channel length. It is evident that by employing long channel TFTs or devices with small channel width, higher gate voltages must be applied in order to reach the maximum OLED brightness at V_{DD} = –4.2 V. The luminance voltage onset is inversely proportional to the channel width-to-length ratio. However, the current density provided by an OET (gated well-above the threshold voltage) is orders of magnitude higher than that required by the light-emitting unit, so that even devices of unlikely low width-to-length ratio (e.g., W/L = 1) can properly drive the OLED at ≈900 cd m^{-2} with low applied gate voltages (|V_{GATE}|< 1 V). Therefore, the pixel addressing circuit can have extremely reduced footprint with respect to the light-emitting unit when OETs are employed. High-resolution light-emitting displays could be fabricated with a simple "parallel-placed" geometry in which both transistors and bottom-emission OLEDs are side-by-side on the same substrate level.

3.3. Dynamic Characteristics and Stability

After characterization of integrated OET/OLED devices in the quasi-equilibrium regime, we determined their response to a dynamic gate bias. The driver TFT was gated with a square wave-function (0 < V_{GATE} < –0.64 V) at different frequencies, while a constant supply bias V_{DD} = –4.2 V was applied between the transistor source and the diode cathode. Consequently, the output of the OLED was modulated in time. In **Figure 6**a,b we report the optical output of a green OLED and the voltage signal applied to the gate of the driving TFT versus time. The gate modulating signal was a square wave-function at 10 Hz

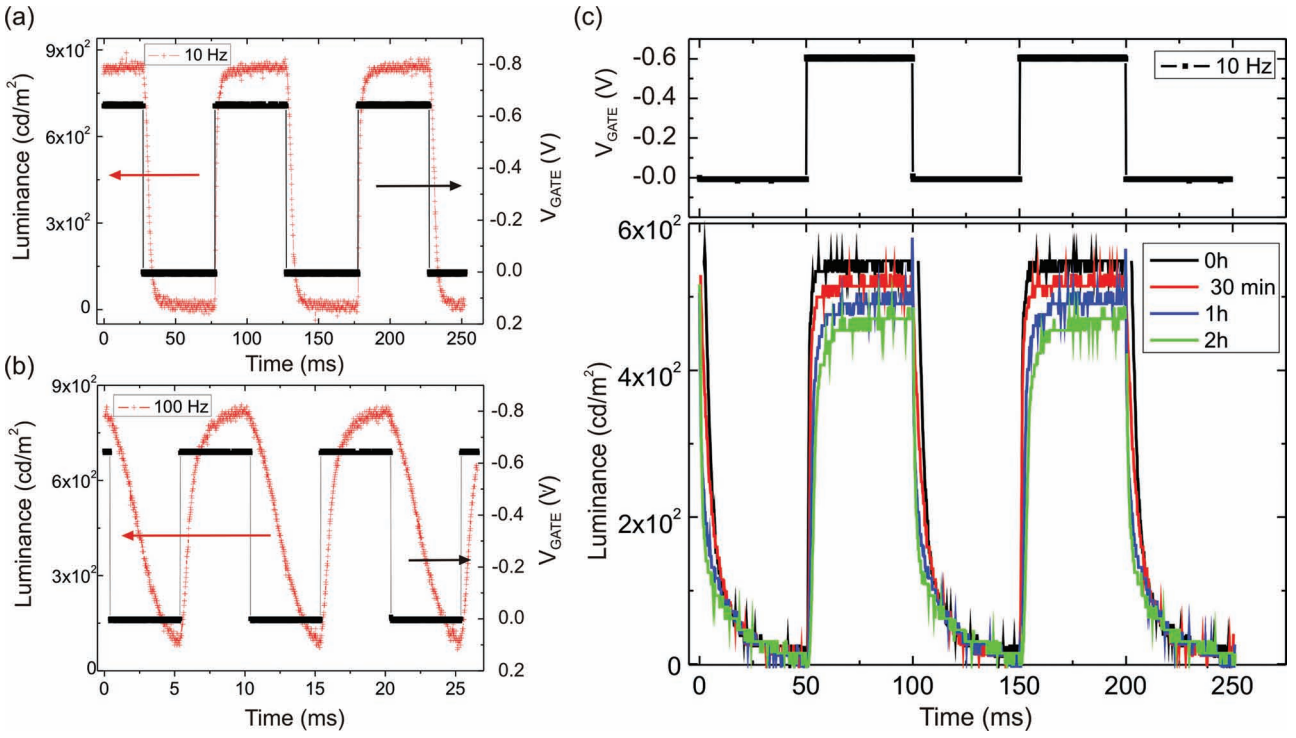

Figure 6. Optical response of an OET/OLED integrated device under dynamic operation. a) Luminance and driving TFT gate voltage vs. time at 10 Hz and b) luminance and TFT gate voltage vs. time at 100 Hz. In both cases the constant supply voltage is $V_{DD} = -4.2$ V. c) Gate stress measurement on an integrated device at switching frequency of 10 Hz and at a constant supply voltage $V_{DD} = -4$ V. The upper and the lower panels report the applied gate voltage and the device optical output versus time, respectively.

(Figure 6a) and 100 Hz (Figure 6b). We note that at 10 Hz the OLED emission perfectly follows the gate signal, switching from a maximum value of ≈900 cd m^{-2} (ON-transistor at V_{GATE} = –0.64 V) to ≈0 cd m^{-2} (OFF-transistor at V_{GATE} = 0 V). Similar behavior is observed when signals with frequencies up to 60 Hz are employed. However, as the frequency increases to 100 Hz, the OLED contrast decreases. The integrated device still responds quickly to the gate signal, but a substantial increase of the OLED brightness during the transistor OFF-state is observed (Figure 6b). Indeed, at high switching frequencies, the OET can still provide enough current to properly drive the OLED, but the device leakage current increases so that the OLED light emission cannot be completely suppressed. The increase of the leakage current is due to less effective electrochemical dedoping of the semiconductor at high switching frequencies (reduced ion diffusion from the channel into the dielectric),[27] and to the contribution of the capacitive current. These effects could be minimized by further optimizing the printing process (giving thinner semiconducting and electrolyte-dielectric layers) and by reducing the dimensions of the source/drain electrodes.

In Figure 6c we report the stability of the integrated devices under dynamic operation. A green OLED was driven by a single OET at a gate switching frequency of 10 Hz and at constant supply voltage $V_{DD} = -4$ V. This is the V_{DD} at which luminance suitable for display applications (≈500 cd m^{-2}) can be achieved with these devices. In order to clearly detect degradations of the device efficiency, the driving transistor was gated at low voltage ($V_{GATE} = -0.6$ V), e.g., close to the voltage edge at which saturation of the driving current occurs. The gate voltage and the luminance of the OLED are reported versus time in the upper and lower panels of Figure 6c, respectively. We note that the integrated device is reasonably stable under bias stress conditions and that after 2 h of dynamic operation the diode optical output still follows properly the gate modulation. Indeed, there are no remarkable changes in the falling and rising edges of the optical signal or in the brightness level of the device OFF-state. However, during the stressing period there is a ≈20% decrease of the maximum OLED luminance. This can be attributed to degradation of both the driving TFT (shift of the threshold voltage and decrease of the total output current) and of the OLED.

4. Active Matrix Organic Light-Emitting Diodes

After the optical/electrical characterization of OLEDs driven by single OETs, we fabricated and characterized all-organic active matrix pixels. G-EML OLEDs of the three additive colors (red, green, and blue (RGB)) were combined with two printed OETs giving simple all-organic light-emitting pixels. We limited our attention to stand-alone pixels, without making an attempt to fabricate a full-color RGB active matrix display. The latter would require complex shadow mask patterning during the OLED fabrication that is beyond the scope of the present work. Moreover, transistors and OLEDs should be isolated with a low-permeability encapsulating layer so as to avoid both performance degradation

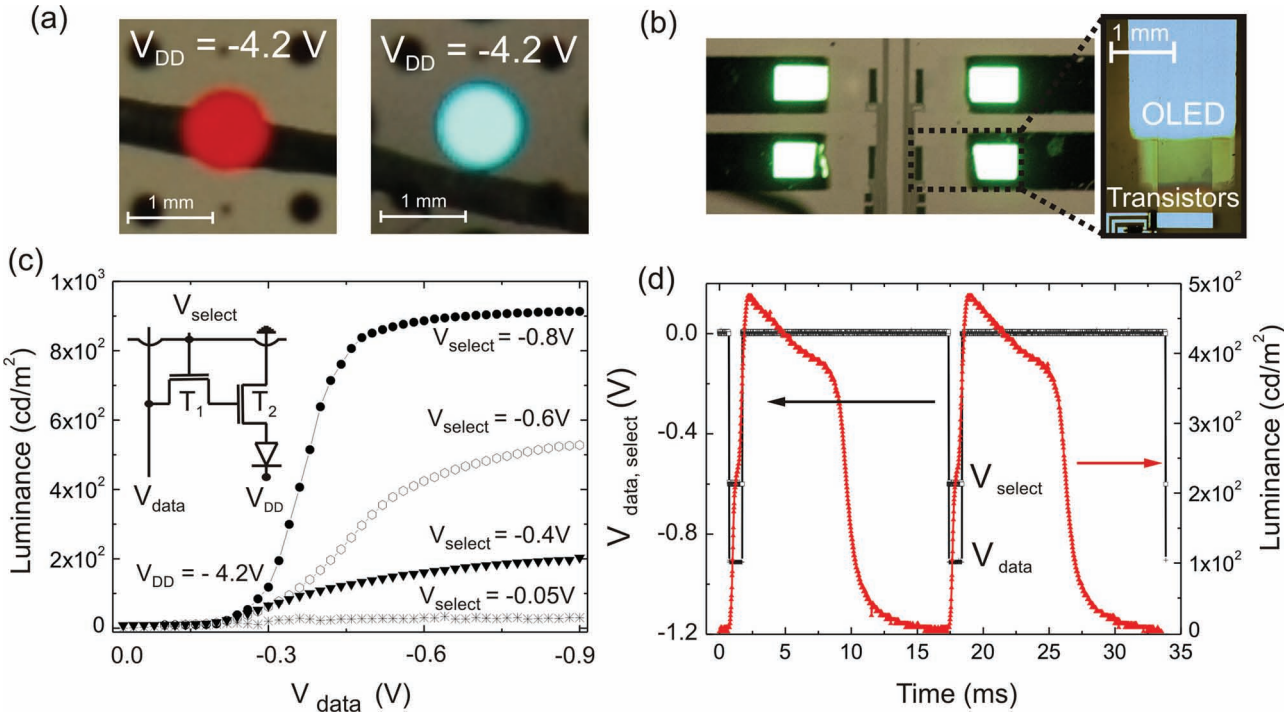

Figure 7. All-organic active matrix red, green, blue light-emitting pixels. a) Photographs of stand-alone red and blue pixels driven by a separate (not integrated) two-transistor circuit and b) green AMOLED pixels integrated with OETs on the same glass substrate. c) Quasi-equilibrium and d) dynamic characteristics of the green pixel at constant supply voltage V_{DD} = –4.2 V. The inset in (c) shows the circuit diagram. T_1 (W = 100 µm, L = 10 µm) and T_2 (W = 200 µm, L = 10 µm) are the switching and the driving transistors, respectively.

by moisture and oxygen and contamination of the OLED by ions from the gate-electrolyte.

Stand-alone red and blue OLEDs were driven by a separate circuit made by two OETs (switcher and driver; **Figure** 7a). Moreover, green AMOLED pixels, composed of the light-emitting unit and two transistors, were integrated on a single glass substrate with lithographically patterned ITO and gold electrodes (the OLED anode and the circuit electrodes, respectively) (Figure 7b). As shown in Figure 7a,b, G-EML OLEDs of the three additive colors can be properly driven by the two-transistor circuit. At a supply voltage V_{DD} = –4.2 V and with sub-1 V gate voltages, brightnesses of ≈900 cd m^{-2} were achieved with green OLEDs, whereas red and blue devices had a maximum luminance of ≈20 cd m^{-2} and ≈400 cd m^{-2}, respectively. Notably, the pixel addressing circuitry has negligible footprint with respect to the dimension of the OLED, as is clear from the magnified picture of a green pixel in Figure 7b. Figure 7c,d show representative quasi-equilibrium and dynamic characteristics of the green OLED pixel shown in Figure 7b. A diagram of the two-transistor circuit we employed is reported in the inset of Figure 7c. T_1 is the switching transistor, i.e., the device that controls writing and holding of data signals (V_{data}) through the applied gate bias (V_{select}), and T_2 is the driving transistor, i.e., the transistor that provides current to drive the OLED. Note that in this simple geometry no storage capacitor is employed. During the pixel dynamic operation, the information (V_{data}) is stored on the parasitic capacitance of the driver TFT. From Figure 7c, where the quasi-equilibrium luminance of the pixel is reported versus V_{data} for different V_{select}, we see that when the switching transistor is fully ON (V_{select} = –0.8 V), the luminance trend is similar to that for the single-transistor integrated device at the same supply voltage V_{DD} = –4.2 V (Figure 3c). Luminance is zero at low applied V_{data} and increases until saturation when the data signal is swept from positive to negative because the data are directly transferred from the switching transistor to the gate of the driving transistor. On the other hand, light emission is suppressed when the gate of the switching transistor is grounded at V_{select} ≈ 0 V. In this case T_1 is OFF and T_2 is isolated from V_{data} so that no dependence of the OLED luminance with respect to V_{data} is observed. The current delivered by the driver to the light-emitting unit is the transistor leakage current at V_{GATE} ≈ 0 V.

In order to simulate the operation of the single pixel in an AMOLED display, we also characterized the device dynamic response (Figure 7d). A pulsed gate bias was applied to the switching OET in order to turn it ON allowing a simultaneous data pulse to be applied to the driver OET gate. V_{select} went from 0 V to –0.6 V, whereas V_{data} from 0 V to –0.96 V. In both cases, the pulse width and the frequency were 1 ms and 60 Hz, respectively. In an active matrix light-emitting display these values would correspond to a 16.7 ms frame time and scan duty factor per line of 1/16. From Figure 7d we see that the pixel responds without significant delay to 1 ms applied pulses and that a considerable brightness level can be reached. However, the device characteristics are clearly not ideal. During dynamic operation, the luminance at V_{DD} = –4.2 V is lower than that

achievable under quasi-static conditions. Also, the data information is not retained during the refreshing period, so that the OLED brightness slowly decreases during the first half of the period and then quickly drops to zero. This is due to the effect of the switching TFT leakage current and to the lack of an additional storage capacitor that could minimize this contribution. However, we believe that improvement of the active matrix dynamic characteristics is possible. Besides optimization of the printing process, SPICE modeling could be used to determine suitable dimensions of transistors and light-emitting unit and the optimal working biases of the circuit. Moreover, more complex voltage-driven active matrix geometries could be employed to reduce both leakage-related issues and the degradation of the transistor/OLED characteristics.[33,35,36]

5. Conclusions

We have shown for the first time that printed OETs can be successfully employed to control high efficiency red, green, and blue AMOLEDs. The OET/OLED all-organic pixels are stable, have high brightness, and have extremely low operation voltage devices in which the driving circuit has reduced area with respect to the OLED. The pixels are operated up to 900 cd m^{-2} with supply voltages near 4 V and sub-1 V driving voltages. These voltages are at least one order of magnitude lower than that required by a light-emitting active matrix in which organic transistors with conventional dielectrics are employed. Essential to this demonstration are the high transconductance of the OETs and the high efficiency/rectifying behavior of the graded emissive layer, phophorescent OLEDs. Collectively, the results suggest that printed OETs, combined with efficient, low voltage OLEDs, could be employed in the fabrication of flexible full-color organic light-emitting displays. Ongoing work will focus on achieving full integration of these devices on flexible substrates and further improving the dynamic response of the pixels by addition of a storage capacitor and minimizing leakage currents.

6. Experimental Section

Device Fabrication: Printed OETs were fabricated with an aerosol jet printer (Optomec Inc.). A chloroform solution of P3HT was printed on top of photolithographically pre-patterned gold source/drain contacts and was covered by sequential printing of an ion gel dielectric layer and a PEDOT:PSS gate electrode. The ion gel was an electronic insulator, made by a gelating triblock copolymer PS-PMMA-PS swollen with a room temperature ionic liquid ([EMIM][TFSI]).[16]

OLEDs were prepared on glass substrates coated with a 150-nm-thick layer of ITO. The composition gradient was achieved by carefully controlling time-varying deposition rates following ref. [26]. Green G-EML OLEDs were fabricated using 4,4′,4″-tris(carbazol-9-yl) triphenylamine (TCTA) and 4,7-diphenyl-1,10-phenanthroline (BPhen) as hole- and electron-transporting host materials, respectively, with the green phosphorescent emitter *fac*-tris(2-phenylpyridine) iridium (III). Red G-EML OLEDs were fabricated using TCTA and BPhen as hole- and electron-transporting host materials, respectively, with the red phosphorescent emitter bis(1-phenylisoquinoline)-(acetylacetonate) iridium (III). Blue G-EML OLEDs were achieved using TCTA and 2,2′,2″-(1,3,5-benzinetriyl)-tris(1-phenyl-1-H-benzimidazole) (TPBi) as hole- and electron-transporting host materials, respectively, with the blue phosphorescent emitter bis(3,5-difluoro-2-(2-pyridyl)phenyl (2-carboxypyridyl)iridium III. Devices with different cathode dimensions were finished by evaporation of LiF and Al through a shadow mask.

Electrical and optical characterizations were performed on stand-alone transistors and OLEDs made on different substrates and electrically connected. Results were also confirmed by testing green pixels fabricated on the same glass substrate. In this case, a two-mask photolithography process was used to pattern the ITO-covered glass substrate and to align the gold electrodes with the ITO-patterns. Different materials for the OLEDs and transistors were then evaporated and printed in succession on the substrate.

Electrical and Optical Measurements: Electrical and optical characterizations were carried out in a nitrogen-filled glove box equipped with two different probe stations. Transistors and OLEDs were characterized in separate probe stations (one of which enabled installation of the photodiode) and then electrically connected to analyze the response of the integrated device. Device quasi-equilibrium electrical characterizations were performed with two Keithley 236 source/measurements units and a Keithley 6517 electrometer. Simultaneously, the optical output of the light-emitting unit were recorded with a Keithley 6517 electrometers connected to a Newport 818-ST calibrated silicon photodetector. In order to characterize the device dynamic response, two Agilent 33220 arbitrary-waveform generators and a Stanford Research SR570 current amplifier connected to a Tektronix TDS1002B were used as input voltage supplies and converting/recording system of the OLED optical signal, respectively.

Acknowledgements

This work was partially supported by the National Science Foundation through the MRSEC program at the University of Minnesota, Award DMR-0819885. The authors acknowledge Keun Hyung Lee for the synthesis of the PS-PMMA-PS. C.D.F. and D.B. also thank the NSF for financial support through award number ECCS-0925312.

Received: September 2, 2011
Revised: October 25, 2011
Published online: February 14, 2012

[1] J.-H. Lee, D. N. Liu, S.-T. Wu, in *Introduction to Flat Panel Displays*, (Eds: A. C. Lowe, M. A. Kriss), Wiley-SID, UK **2008**.
[2] G. P. Crawford, *Flexible Flat Panel Display*, Wiley-SID, UK **2005**.
[3] G. Gelinck, P. Heremans, K. Nomoto, T. D. Anthopoulos, *Adv. Mater.* **2010**, *22*, 3778.
[4] H. Sirringhaus, N. Tessler, R. H. Friend, *Science* **1998**, *280*, 1741.
[5] A. Dodabalapur, Z. Bao, A. Makhija, J. G. Laquindanum, V. R. Raju, Y. Feng, H. E. Katz, J. Rogers, *Appl. Phys. Lett.* **1998**, *73*, 142.
[6] C. D. Sheraw, L. Zhou, J. R. Huang, D. J. Gundlach, T. N. Jackson, M. G. Kane, I. G. Hill, M. S. Hammond, J. Campi, B. K. Greening, J. Francl, J. West, *Appl. Phys. Lett.* **2002**, *80*, 1088.
[7] H. E. A. Huitema, G. H. Gelinck, J. B. P. H. van der Putten, K. E. Kuijk, C. M. Hart, E. Cantatore, P. T. Herwig, A. J. J. M. van Breemen, D. M. de Leeuw, *Nature* **2001**, *414*, 599.
[8] J. A. Rogers, Z. Bao, K. Baldwin, A. Dodabalapur, B. Crone, V .R. Raju, V. Kuck, H. Katz, K. Amundson, J. Ewing, P. Drzaic, *Proc. Natl. Acad. Sci. USA* **2001**, *98*, 4835.
[9] G. H. Gelinck, H. E. A. Huitema, E. Van Veenendaal, E. Cantatore, L. Schrijnemakers, J. B. P. H. Van der Putten, T. C. T. Geuns, M. Beenhakkers, J. B. Giesbers, B.-H. Huisman, E. J. Meijer, E. Mena Benito, F. J. Touwslager, A. W. Marsman, B. J. E. Van Rens, D. M. De Leeuw, *Nat. Mater.* **2004**, *3*, 106.
[10] P. Andersson, R. Forchheimer, P. Tehrani, M. Berggren, *Adv. Funct. Mater.* **2007**, *17*, 3074.

[11] L. Zhou, A. Wanga, S.-C. Wu, J. Sun, S. Park, T. N. Jackson, *Appl. Phys. Lett.* **2006**, *88*, 083502.
[12] I. Yagi, N. Hirai, M. Noda, A. Imaoka, Y. Miyamoto, N. Yoneya, K. Nomoto, J. Kasahara, A. Yumoto, T. Urabe, *Proc. Soc. Inf. Disp.* **2007**, *38*, 1753.
[13] T. Sekitani, H. Nakajima, H. Maeda, T. Fukushima, T. Aida, K. Hata, T. Someya, *Nat. Mater.* **2009**, *8*, 494.
[14] T. Suzuki, *J. Appl. Phys.* **2006**, *99*, 111101.
[15] M. G. Kane, in *Organic Field-Effect Transistors*, (Eds: Z. Bao, J. Locklin), CRC Press, Boca Raton, FL **2007**, Ch. 6.4.
[16] J. H. Cho, J. Lee, Y. Xia, B. Kim, Y. He, M. J. Renn, T. P. Lodge, C. D. Frisbie, *Nat. Mater.* **2008**, *7*, 900.
[17] S. Chao, M. S. Wrighton, *J. Am. Chem. Soc.* **1987**, *109*, 2197.
[18] J. T. Mabeck, G. G. Malliaras, *Anal. Bioanal. Chem.* **2006**, *384*, 343.
[19] L. Herlogsson, X. Crispin, N. D. Robinson, M. Sandberg, O.-J. Hagel, G. Gustafsson, M. Berggren, *Adv. Mater.* **2007**, *19*, 97.
[20] T. Mills, L. G. Kaake, X.-Y. Zhu, *Appl. Phys. A* **2009**, *95*, 291.
[21] Y. Xia, W. Zhang, M. Ha, J. H. Cho, M. J. Renn, C. H. Kim, C. D. Frisbie, *Adv. Funct. Mater.* **2010**, *20*, 587.
[22] M. Ha, Y. Xia, A. A. Green, W. Zhang, M. J. Renn, C. H. Kim, M. C. Hersam, C. D. Frisbie, *ACS Nano* **2010**, *4*, 4388.
[23] K. H. Lee, S. Zhang, T. P. Lodge, C. D. Frisbie, *J. Phys. Chem. B* **2011**, *115*, 3315.
[24] H. Matsumoto, *Electrochemical Aspects of Ionic Liquids*. Wiley, Hoboken, NJ **2005**.
[25] N. D. Robinson, P.-O. Svensson, D. Nilsson, M. Berggren, *J. Electrochem. Soc.* **2006**, *153*, 39.
[26] N. C. Erickson, R. J. Holmes, *Appl. Phys. Lett.* **2010**, *97*, 083308.
[27] J. Lee, L. G. Kaake, J. H. Cho, X.-Y. Zhu, T. P. Lodge, C. D. Frisbie, *J. Phys. Chem. C* **2009**, *113*, 8972.
[28] D. Braga, M. Ha, W. Xie, C. D. Frisbie, *Appl. Phys. Lett.* **2010**, *97*, 193311.
[29] L. Herlogsson, Y. Y. Noh, N. Zhao, X. Crispin, H. Sirringhaus, M. Berggren, *Adv. Mater.* **2008**, *20*, 4708.
[30] M. L. Chabinyc, A. Salleo, *Chem. Mater.* **2004**, *16*, 4509.
[31] J.-C. Goh, H.-J. Chung, J. Jang, C.-H. Han, *IEEE Electron Devices Lett.* **2002**, *23*, 544.
[32] A. A. Orouji, M. J. Kumar, *IEEE Trans. Device Mater. Reliab.* **2006**, *6*, 315.
[33] C.-W. Lin, M. C.-T. Chao, Y.-S. Huang, *IEEE Trans. VLSI* **2010**, *19*, 939.
[34] J.-H. Lee, H.-S. Park, J.-H. Jeon, M.-K. Han, *Solid-State Electron.* **2008**, *52*, 467.
[35] C.-L. Lin, Y.-C. Chen, *IEEE Electron. Devices Lett.* **2007**, *28*, 229.
[36] H.-S. Park, W. Lee, S.-H. Kuk, M.-K. Han, *ECS Trans.* **2007**, *8*, 65.